Surfactant Limited Aggregation of Hydrophobic Molecules in Water

Hélène Lannibois, Anwar Hasmy, Robert Botet, Olivier Chariol, Bernard Cabane

▶ **To cite this version:**

Hélène Lannibois, Anwar Hasmy, Robert Botet, Olivier Chariol, Bernard Cabane. Surfactant Limited Aggregation of Hydrophobic Molecules in Water. Journal de Physique II, 1997, 7 (2), pp.319-342. 10.1051/jp2:1997128 . jpa-00248446

HAL Id: jpa-00248446
https://hal.science/jpa-00248446

Submitted on 4 Feb 2008

HAL is a multi-disciplinary open access archive for the deposit and dissemination of scientific research documents, whether they are published or not. The documents may come from teaching and research institutions in France or abroad, or from public or private research centers.

L'archive ouverte pluridisciplinaire **HAL**, est destinée au dépôt et à la diffusion de documents scientifiques de niveau recherche, publiés ou non, émanant des établissements d'enseignement et de recherche français ou étrangers, des laboratoires publics ou privés.

J. Phys. II France 7 (1997) 319–342 FEBRUARY 1997, PAGE 319

Surfactant Limited Aggregation of Hydrophobic Molecules in Water

Hélène Lannibois ([1]), Anwar Hasmy ([2]), Robert Botet ([2,*]), Olivier Aguerre Chariol ([3]) and Bernard Cabane ([1])

([1]) Equipe mixte CEA - RP, Rhône-Poulenc, 93308 Aubervilliers, France
([2]) Laboratoire de Physique des Solides, Université Paris-Sud, Bâtiment 510, 91405 Orsay, France
([3]) Rhône-Poulenc, 93308 Aubervilliers, France

(Received 28 July 1996, received in final form 11 October 1996, accepted 25 October 1996)

PACS.82.70.Kj – Emulsions and suspensions
PACS.82.20.Wt – Computational modeling; simulation
PACS.05.40.+j – Fluctuation phenomena, random processes, and Brownian motion

Abstract. — The precipitation in water of hydrophobic molecules has been studied in presence of added surfactants. Amorphous particles grow through aggregation of clusters of hydrophobic molecules; the growth is terminated by adsorption of surfactant. The particle sizes vary according to the concentrations of hydrophobic molecules and of surfactant molecules. Two regimes have been found for the use of surfactant molecules: at low surfactant concentrations, an efficient regime where all surfactant molecules are adsorbed on the surfaces of the growing particles; at high surfactant concentrations, a wasteful regime, where excess surfactant molecules are left in water. Attempts to reduce the particle sizes by adding increasing amounts of surfactant become inefficient at some point where most of the added surfactant remains in water. These results are explained by a kinetic aggregation model which simulates the competition between aggregation of hydrophobic molecules and adsorption of surfactant. The results of experiments are well reproduced by simulations where aggregation is allowed to proceed unimpeded for a time τ, and then adsorption of the surfactant starts. In these conditions, particle sizes are determined by the rate of aggregation and by the value of this time delay.

1. Introduction

Many drugs currently under development are made of large hydrophobic molecules. In order to reach the active sites, these molecules must be carried across an aqueous environment. However, the amount of drug that can be dissolved and transported in the aqueous medium is much too low for practical purposes: typical solubilities for large hydrophobic molecules range from 10^{-8} g/g to 10^{-5} g/g. The classical way to achieve this transport is to dissolve the hydrophobic molecules into carrier particles, *i.e.* supramolecular objects which may be dispersed in water. Typical carriers are polymeric particles, liposomes, micelles [1–4]. Still, the amount of drug that can be dissolved in most carriers is small, about 10% of the carriers mass. Therefore there is a need to design a carrier free delivery system, where particles of

(*) Author for correspondence (e-mail: botet@lps.u-psud.fr)

© Les Éditions de Physique 1997

pure drug could be covered with a small amount of surfactant and dispersed in water. The requirements are that the particle size should be smaller than 0.2 μ, the specific surface area should be of the order of 100 m^2/g, and the amount of surfactant should be as low as possible.

Very fine dispersions may be obtained, either by fragmentation [5–8], or by growth processes [9,10]. In fragmentation, particles of hydrophobic products may be produced by emulsification of the product in water, if it is a liquid, or grinding it down to a very small size, if it is a solid. In growth processes, the hydrophobic product is dissolved in a solvent that is miscible with water, and then the solution is mixed with water, causing the insoluble molecules to precipitate. It is then necessary to control the precipitation process to obtain colloidal particles instead of a macroscopic solid.

In all these processes, surfactants are needed, either to help the fragmentation (emulsification of grinding) or to prevent aggregation of the fragmented particles, or to control growth. The problem is that the necessary amounts of surfactant are large, sometimes comparable with the amount of hydrophobic product. This reduces the advantage of such delivery systems over the traditional carriers, and may cause a non specific toxicity of the formula. In this paper, we address the problem of the use of surfactants for one particular case: dispersions made through a precipitation process.

We consider a "model" hydrophobic product made of molecules that are nearly insoluble in water (10^{-8}g/g). This hydrophobic product is dissolved in a solvent that is miscible with water, and the solution is mixed with a large excess of water. The hydrophobic molecules are instantly desolvated. Because they are insoluble in water, they stick to each other whenever they meet, and dissociation reactions do not occur. In such conditions, there is no nucleation barrier, and aggregates of hydrophobic molecules grow immediately through a Diffusion Limited Cluster-cluster Aggregation (DLCA) mechanism [11–13].

If this aggregation is allowed to continue, the aggregates will become so large that they will reach macroscopic sizes and fall out of solution (precipitation). However, surfactants may be added in order to control this growth. Indeed, surfactant molecules may adsorb on the growing aggregates through their hydrophobic tails. Hydrophobic surfaces that are fully covered with surfactant may not stick to each other; hence, aggregates that are saturated with surfactant molecules will no longer recombine with other aggregates. In this way, a stable dispersion of nanometric aggregates may be obtained.

This description of a poisoned aggregation process suggests that the amount of surfactant needed to control the final sizes of the aggregates should be the amount which covers their surfaces. As will be shown below, the aggregates are often spherical, amorphous particles, because their interior is platicized by residual solvent and water. Therefore a monolayer coverage by adsorbed surfactant would require a ratio of surfactant volume (V_S) to hydrophobic volume (V_H) volume given by:

$$\frac{V_S}{V_H} = \frac{3r}{R} \tag{1}$$

where r is the thickness of the surfactant layer and R the radius of the particles. Typically, the desired particle diameters are 100 nm, and thus the ratio V_S/V_H should be of the order of 0.06. However, a general finding is that the amount of surfactant needed to control the growth of aggregates in such conditions is vastly in excess of a monolayer coverage. This inefficient use of surfactants may have two possible origins: either the surfactant molecules are not available near the particle surfaces during the aggregation process, or they are available, but they do not protect the surfaces efficiently.

In the following, we report the formation of nanoparticles by aggregation of hydrophobic molecules in presence of surfactants; different conditions have been set for the competition between aggregation and poisoning by surfactants, and the resulting particle sizes have been

measured. In order to interpret these data, we have designed a kinetic model where hydrophobic molecules and surfactants (or poisons) are moved at random on a lattice. The process of poisoned aggregation has been reproduced with a set of rules that determine the sticking probabilities of all species. This simulation shows two regimes for the use of surfactants: an "efficient" regime, where the surfactant molecules are used efficiently, but the aggregation proceeds to rather large sizes, and a "wasteful" regime, where a vast excess of surfactant is used to stop the aggregation at an earlier stage. The comparison with experimental results shows that the preparation of nanoparticles is usually conducted in the "wasteful" regime where a large fraction of the surfactant remains in the aqueous phase. Dispersions of nanometric particles (sizes below 100 nm) cannot be obtained in the "efficient" regime, unless the surfactant adsorbs more efficiently on the growing aggregates than the hydrophobic molecules themselves.

2. Materials

The hydrophobic product used in most precipitation experiments was cholesteryl acetate. This product was chosen because it has a very low solubility in water (2×10^{-8} g/g), a substantial solubility in polar solvents that are miscible with water (*e.g.* 0.034 g/g in acetone at 23 °C), and because it resembles a number of drugs currently in development. It is a solid (mp = 115 °C) which can be obtained in a number of crystal structures [14–16], or in an amorphous or microcrystalline state.

We also used a liquid hydrophobic product, hexadecane (mp = 18 °C), in order to compare the sizes of particles prepared through precipitation and through emulsification. The solubility of hexadecane in water is 1×10^{-11} g/g.

For neutron scattering experiments, intended to determine the location of the surfactant, we used deuterated polystyrene to make the cores of the hydrophobic nanoparticles. This polymer was a generous gift from Claude Picot at the Institut Charles Sadron; it had an average molar mass $M = 15000$ g/mol. It is noted hereafter PSD.

The surfactants used in this study were an ethoxylated fatty alcohol with 12 carbons in the linear alkyl chain and 5 oxyethylene groups, hereafter named $C_{12}E_5$, and a diblock copolymer made of a styrene block (molar mass 1000) and an oxyethylene block (molar mass 1000), hereafter named PS-POE. This polymer was obtained from Goldschmidt (type VPSE 1010). When these surfactants are adsorbed from a micellar solution on a hydrophobic surface, they form monolayers where the area per surfactant molecule is 0.48 nm^2 for $C_{12}E_5$ and 1.28 nm^2 for PS-POE; the thickness of these layers are 0.5 nm and 2.5 nm, respectively.

The hydrophobic molecules were initially dissolved in polar solvents which were acetone (for cholesteryl acetate with PSPOE), ethanol (for hexadecane and $C_{12}E_5$) and tetrahydrofuran (THF) (for PSD and PS-POE).

The variables which define the composition of the mixtures are c_H, initial concentration of hydrophobic molecules in the solvent, and c_S, initial concentration of surfactant in the solvent. Both are expressed in g/g. It was found that the outcome of the precipitation is mainly determined by the value of the ratio c_S/c_H. Typical values for the composition were: c_H, 10^{-3} to 3×10^{-2} g/g; ratio c_S/c_H, 5×10^{-3} to 10; final concentration of hydrophobic molecules in water, 10^{-5} to 3×10^{-3} g/g; final concentration of solvent in water, 10^{-2} g/g.

3. Methods

3.1. PRECIPITATION. — The precipitation of hydrophobic molecules in water was performed as follows. First, the hydrophobic product and the surfactant were dissolved in the polar solvent. Then the solution was injected into a large volume of water. At the moment of injection,

the local supersaturation of hydrophobic molecules was on the order of 10^5. This very high supersaturation caused immediate aggregation of the hydrophobic molecules, as described in the introduction. The aggregation stopped at a stage that was determined by the relative concentrations of hydrophobic molecules, c_H, and of surfactant, c_S. The final dispersion had colloidal stability in all cases, excepted for hexadecane droplets covered with a very small amount of surfactant.

3.2. QUASI ELASTIC LIGHT SCATTERING. — The sizes of the particles in the final dispersion were calculated from their motions measured through Quasi Elastic Light Scattering (QELS) [17,18]. It was found that the sizes were in the range 50 to 500 nm, for which this method is adequate.

3.3. SMALL ANGLE NEUTRON SCATTERING. — The structures of the particles were examined through SANS [17, 18]. Neutrons are scattered by differences in scattering length between nuclei in the particles and nuclei in the continuous phase. Good contrast between particles and continuous phase was achieved using D_2O as the continuous phase. This contrast was used to determine whether the particles were porous or dense. Alternatively, the hydrophobic molecules and water were deuterated, while the surfactant remained hydrogenated. This contrast was used to determine the location and the structure of the surfactant within the particles. Two-dimensional scattering patterns were obtained on the instrument D11 at ILL. These patterns were subsequently radially averaged to yield scattering curves of intensity, I, *vs.* magnitude, Q, of the scattering vector. Q is related to the wavelength, λ, of incident neutrons and to the scattering angle, θ, by:

$$Q = \frac{4\pi}{\lambda} \sin\left(\frac{\theta}{2}\right). \tag{2}$$

The general features of scattering curves for independent particles dispersed in a homogeneous continuous phase are as follows [19]:

(a) at $Q \to 0$ the intensity, I_o, is proportional to particle mass concentration and to the square of the difference in density of scattering length, $\Delta\rho$, between D_2O and the protonated molecules in the particles. Hence, the average content of the particles may be determined;

(b) at low Q values, the rays scattered by nuclei at opposite ends of the particle interfere destructively. In this regime, the curvature of the scattering curve measures the average radius of gyration, R_g, of the particles. This quantity may be determined by fitting the measured intensity curve to an expansion formula. For globular particles the best expansion is the Guinier formula:

$$I(Q) = I_o \exp\left(-\frac{Q^2 R_g^2}{3}\right); \tag{3}$$

(c) at higher Q values, the intensity decay reflects interferences at shorter distances within each particle, *i.e.* their internal structure. For dense globular particles (no internal structure), the intensity follows Porod's law, from which the surface area A of the particles may be determined:

$$I(Q) \approx AQ^{-4} \tag{4}$$

For flat particles or hollow shells, the destructive interference is not as strong, and the decay is only according to Q^{-2}; for rod-like particles it is Q^{-1} For bushy or porous particles with fractal dimension d_f the decay follows the power law Q^{-d_f} Thus, from the slope of the intensity decay in a log-log plot, the dimensionality of the particles may be determined.

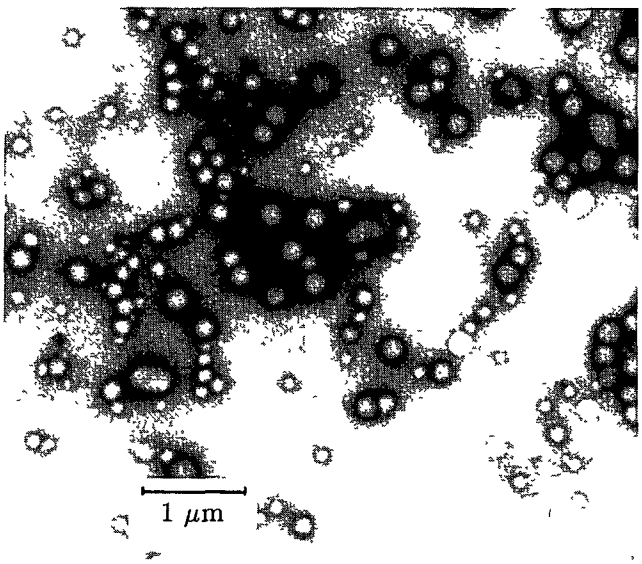

Fig. 1. — TEM image of a cholesteryl acetate dispersion in water. Uranyl acetate was added to the dispersion, then it was dried in air on a collodion membrane before observation; this caused the aggregation of most particles, and the recrystallization of a few.

3.4. Electron Microscopy. — The particle shapes and sizes were also observed through Cryo-Transmission Electron Microscopy (CRYO-TEM) [20]. Thin liquid films were prepared on perforated carbon films supported on 3 mm electron microscope grids. A specimen was prepared by applying a small (about 3 μl) drop onto the grid, blotting most of it to the desired thickness (under 200 nm) and plunging it into liquid ethane at its melting point. This ultra-fast cooling caused vitrification of the liquid phase, *i.e.*, specimens became solid-like (vitreous) without change of phase that leads to structural rearrangement. These cryo-specimens were stored under liquid nitrogen, and transferred to the cooling-holder (Gatan 626) of the TEM (JEOL 2000FX), where they were equilibrated at −170 °C, and examined with an acceleration voltage of 100 kV.

3.5. Composition Variables. — All these measurements were performed in order to study how surfactants limit the aggregation process and the loss of surface area that results from the aggregation. The results are expressed in two ways: first, as an average particle volume V_{av}; second, as a normalized surface area, *i.e.* the total surface area of the dispersion divided by the surface area that would be created if all the surfactant molecules were used to cover the particle surfaces. These quantities are measured in the final dispersions, made at different values of the composition variables c_H, c_S, or c_S/c_H; the laws for these variations are then compared with the laws predicted by the kinetic growth models.

4. Experimental Results

4.1. Observation of the Dispersions Through Electron Microscopy. — In a first step, cholesteryl acetate dispersions were dried on a collodion membrane and examined through TEM. The image (Fig. 1) shows a collection of globular particles, with sizes in the 100 nm range, and a broad distribution of sizes. It can also be seen that extensive aggregation and

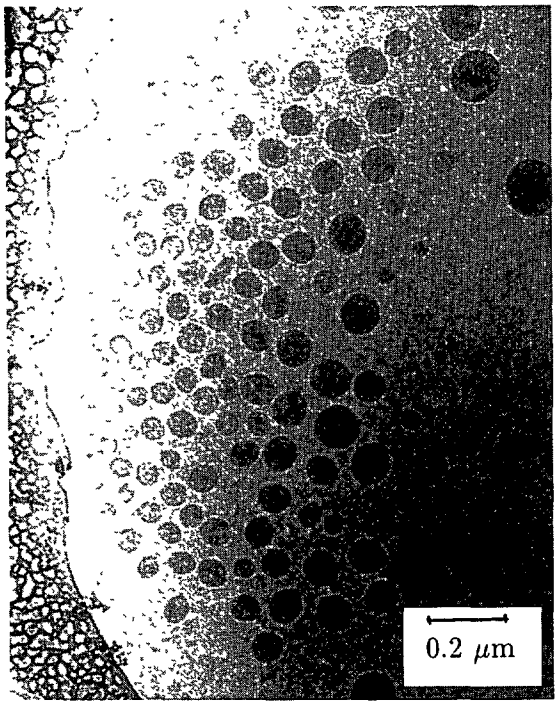

Fig. 2. — CRYO-TEM image of a cholesteryl acetate dispersion in water with PS-POE as a surfactant ($c_H = 10^{-2}$ g/g and $c_S/c_H = 0.1$). The film of vitrified water appears as a uniform grey background. This film is held across a perforation in a carbon film, which is also seen. The cholesteryl acetate particles are in the vitrified water film, pushed by the meniscus against the edge of the film. The important features are the good dispersion of the particles in water, their globular shapes and the absence of any crystallinity.

some recrystallization have occurred as a result of drying. All subsequent examination of the dispersions were made through CRYO-TEM. The image shown in Figure 2 shows particles confined in the meniscus of the vitrified water film, near the edge of one of the perforations in the carbon film. The particles appear non-aggregated, with an amorphous structure and globular shapes. This was confirmed in every observation through CRYO-TEM. A measurement of the particle sizes (diameters) was performed on an image where the particles were uniformly dispersed in the vitrified water film; the resulting size distribution is shown in Figure 3.

4.2. Systematic Study of Particle Sizes. — In a first set of experiments, the hydrophobic molecules were cholesteryl acetate and the surfactant was the diblock copolymer PS-POE. Both were dissolved in acetone, and the solution was precipitated in water. The initial concentrations were: cholesteryl acetate, 10^{-2} g/g; PS-POE, 5×10^{-4} to 10^{-2} g/g; the final concentrations were 100 times smaller. A colloidal dispersion was obtained in every case. The sizes of the particles in the dispersion were measured immediately through QELS, and then again at later times. It was found that these sizes remained the same over more than one month. Figure 4 shows the average particle volumes calculated from these radii, at $c_S/c_H = 1$, for different values of the initial concentration c_H of cholesteryl acetate in acetone.

The radii vary between 15 and 30 nm, and the volumes between 14×10^3 and 110×10^3 nm^3, for the initial concentration $c_H = 10^{-2}$ g/g. They are always larger than the volumes that

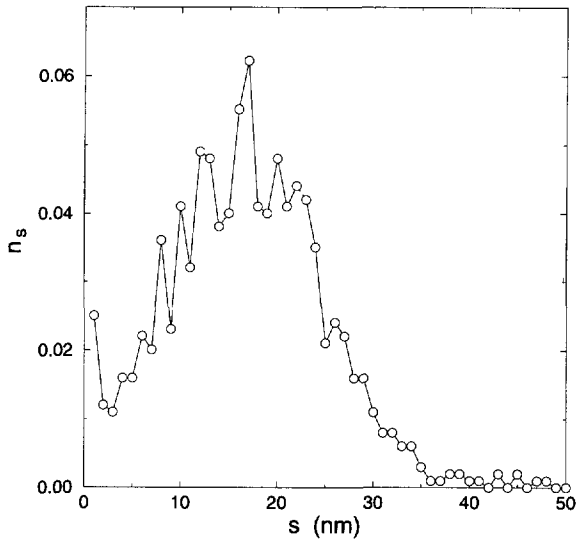

Fig. 3. — Distribution of particle sizes (diameters) n_s measured on a CRYO-TEM image ($c_H = 10^{-2}$ g/g and $c_S/c_H = 1$). The image contained 1000 particles, uniformly distributed across the film of vitrified water. The particles were selected individually and their diameters s were then measured automatically by a computer program.

would be obtained if all the surfactant had been used to limit aggregation by covering the particle surfaces: at $c_S/c_H = 1$, the particle volume corresponding to an efficient use of the surfactant would be 4000 nm^3. At high dilution, the particle volumes approach the limit of efficient use of surfactant, and they rise away from it when the concentration c_H of hydrophobic molecules is increased. The law for this rise was found to be the same at all compositions c_S/c_H of this system; it is:

$$V_{av} \propto c_H. \tag{5}$$

Other experiments were performed with hexadecane as a hydrophobic molecule, and $C_{12}E_5$ as a surfactant, both dissolved in ethanol. At high surfactant concentration ($c_S/c_H = 1$ and $c_S/c_H = 0.4$), the measured volumes were larger than those of cholesteryl acetate particles, and much larger than the volumes calculated for an efficient use of surfactant; again, they follow the law described in equation (5). However, at low surfactant concentration ($c_S/c_H = 0.04$), two successive regimes were observed: at large dilutions ($c_H < 10^{-2}$ g/g) a regime of efficient use of the surfactant (denoted by arrows in Fig. 4), and at higher concentrations, again the regime of wasteful use of the surfactant (rising straight line in the log-log representation of Fig. 4).

In summary, the particle volumes are generally larger than those predicted for an efficient use of the surfactant, and they rise with the concentration of hydrophobic molecules in the initial solution, according to equation (5).

We have also measured systematically the particle volumes obtained with the same initial dilution c_H but different values of the ratio c_S/c_H (Fig. 5). The data for hexadecane and $C_{12}E_5$ show a fast decrease of the average volumes at $c_S/c_H < 0.05$, indicating that the surfactant is used efficiently, followed by a slow decrease at $c_S/c_H > 0.05$, indicating that the additional surfactant is mostly wasted.

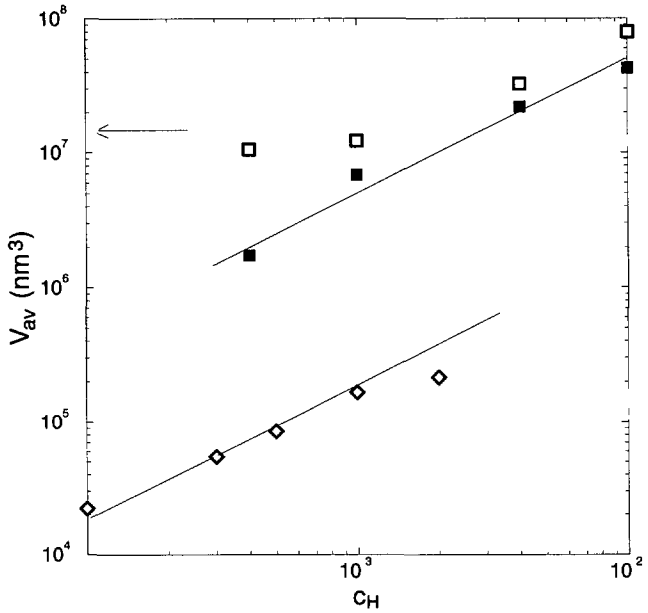

Fig. 4. — Average particle volumes V_{av} measured through QELS. Each set of data corresponds to dispersions made from the precipitation of solutions containing a given hydrophobic product and surfactant; the ratio c_S/c_H of surfactant to hydrophobic molecules has been kept a constant, but the overall dilution of the solution, measured by c_H, has been changed. Hollow diamonds: cholesteryl acetate and PS-POE, at $c_S/c_H = 1$. Filled squares: hexadecane and $C_{12}E_5$ at $c_S/c_H = 0.4$. Hollow squares: hexadecane and $C_{12}E_5$ at $c_S/c_H = 0.04$. The arrow indicates the values of the volumes calculated for an efficient use of the surfactants, and the filled lines are a linear fit through the data. The slope of the data is 1 in log-log scales, as predicted by a kinetic aggregation model.

In order to put these notions of efficient or wasteful use of the surfactant on a quantitative basis, it is useful to calculate the amount of particle surface that has been protected from aggregation by the adsorption of surfactant. The surface area of the particles may be calculated from their radii, assuming a globular shape. If the surfactant was used efficiently, this surface area would equal the surface area of a monolayer containing all the surfactant molecules. Thus the ratio of both quantities is an indicator of the effectiveness of the surfactant. The values of this ratio are presented in Figure 6.

For hexadecane droplets covered by $C_{12}E_5$, we choose a surface area of 0.47 nm^2 per surfactant molecule [21, 22]. The calculated ratios show a regime of efficient use up to $c_S/c_H = 0.05$, followed by a wasteful regime. For cholesteryl acetate particles covered by PS-POE, we choose a surface area of 1.28 nm^2 per surfactant molecule [23]. The calculated ratios show a regime where, surprisingly, more surface is kept than what is covered by the surfactant. In fact, cholesteryl acetate particles can be obtained in the absence of any added surfactant. This is because cholesteryl acetate contains ionic impurities that cause the particles to repel each in any medium where ionic dissociation is possible. Therefore the cholesteryl acetate dispersions are always in the regime of excess surfactant.

In summary, it is not possible to obtain particles of arbitrarily small volumes by adding sufficient amounts of surfactant: in such cases, only a small fraction of the surfactant is efficient in controlling the aggregation. This result cannot be improved unless one understands the fate of the wasted surfactant; this is one of the goals of the next section.

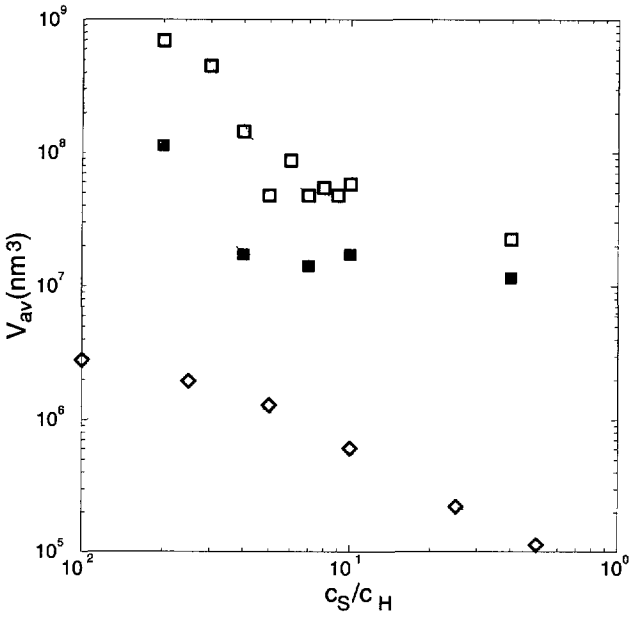

Fig. 5. — Effect of surfactant concentration c_S on the average particle volumes V_{av}. Each set of data corresponds to dispersions made from the precipitation of solutions containing a given hydrophobic product and surfactant; the overall dilution of the solution, measured by c_H, has been kept a constant, but the ratio c_S/c_H of surfactant to hydrophobic molecules has been changed. Hollow diamonds: Cholesteryl acetate and PS-POE, at $c_H = 0.01$ g/g. Filled squares: hexadecane and $C_{12}E_5$ at $c_H = 0.04$ g/g. Hollow squares: hexadecane and $C_{12}E_5$ at $c_H = 0.1$ g/g. The lines are a guide to the eye.

4.3. Structures of Particles and Location of the Surfactant. — The process of poisoned aggregation can also be characterized according to the structures and to the composition of the final aggregates. This is interesting for a number of reasons.

• The aggregation of colloidal particles through Diffusion Limited Aggregation of Clusters (DLCA) usually produces aggregates with fractal or porous structures [11–13]. Are such tenuous structures preserved in the final particles, or is there a reordering process by which the voids collapse and the structures become dense?

• The amount of hydrophobic surface that is calculated from the particle radii is usually much less than the amount that should have been protected by the adsorption of surfactant (see the previous Sect.). Where is the wasted surfactant: has it been trapped inside the particles by the reordering of subunits, or did it remain in the aqueous phase for kinetic reasons?

Quantitative answers to these questions were obtained through SANS, using the appropriate contrasts to observe either the scattering from hydrophobic molecules and surfactants, or from surfactants alone.

A first set of experiments was performed with particles made of cholesteryl acetate, with or without PS-POE as a surfactant, in an aqueous phase made of D_2O. In this case the contrast is between water and all the molecules that form the nanoparticles. These scattering curves are shown in Figure 7: they show an initial downward curvature followed by a steep decay. The initial curvature is related to the particle sizes according to equation (3); the sizes measured

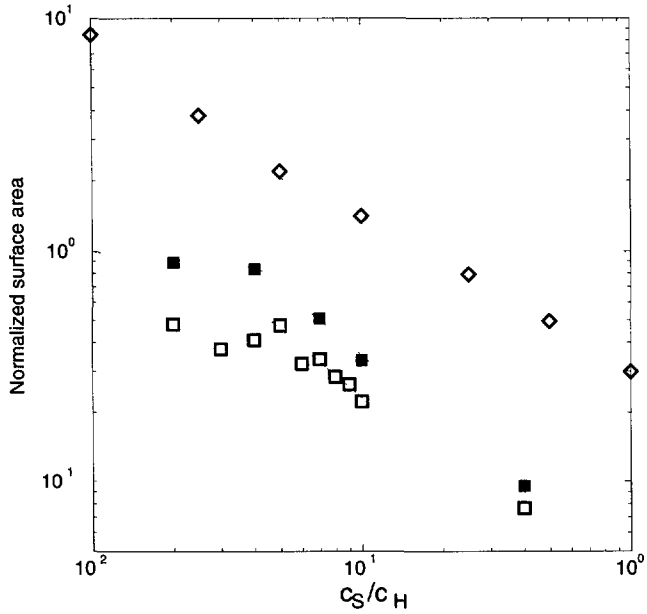

Fig. 6. — Surface area of the particles, divided by the surface area that would be kept if all surfactant molecules were adsorbed on the particle surfaces. Hollow diamonds: Cholesteryl acetate and PS-POE, at $c_H = 0.01$ g/g. Filled squares: hexadecane and $C_{12}E_5$ at $c_H = 0.04$ g/g. Hollow squares: hexadecane and $C_{12}E_5$ at $c_H = 0.1$ g/g. The lines are a guide to the eye. Efficient use of the surfactant would yield a surface area ratio equal to unity. Lower values indicate that some surfactant is wasted; higher values indicate that other forces besides the adsorption of surfactant limit the aggregation process.

through a fit of the scattering curves in this range of Q are in good agreement with those obtained from QELS. The steep decay is related to the shape of the particles: according to equation (4), the Q^{-4} power law indicates that the particles are dense. Therefore, aggregation events must be followed by a reordering process that collapses the voids to give dense structures.

A second set of experiments was performed with particles made of PSD, using PS-POE as a surfactant, in an aqueous phase made of D_2O. In this case the contrast is between the hydrogenated surfactant and the deuterated aqueous phase. The scattering curves obtained at high ratios of surfactant to hydrophobic molecules ($c_S/c_H = 0.5$ or 1) show a Q^{-2} decay, and a characteristic shoulder near $Q = 0.3$ nm^{-1} (Fig. 8). The scattering curves of samples made at low ratios ($c_S/c_H = 0.05$ to 0.25) show the same initial power law decay, but the shoulder has vanished (Fig. 8).

A transcription of these features into real space is as follows. The Q^{-2} power law of the initial decay comes from flat structures such as hollow shells. The shoulder at $Q = 0.3$ nm^{-1} shows that there are other objects that also contribute to the scattering; these objects have a size on the order of $1/Q$. A fit of the scattering curve is obtained by adding the scattering from flat objects (Q^{-2} power law) and the scattering from small spheres with a diameter of 7.6 nm.

These features are observed in dispersions where the coherent scattering is caused by the surfactant molecules only. In terms of the location of the surfactant molecules, the interpretation is as follows. The hollow shells are surfactant monolayers that cover the nanoparticles.

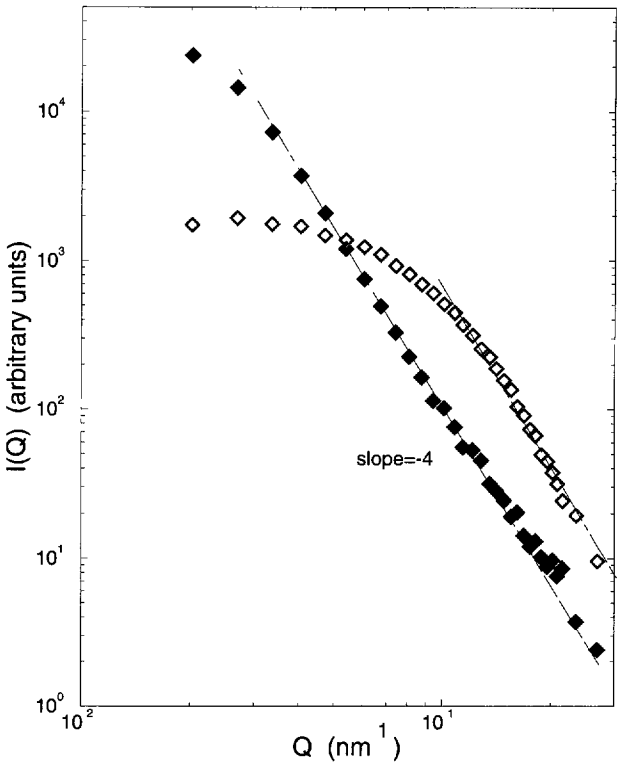

Fig. 7. — Small Angle Neutron Scattering curves of dispersions containing cholesteryl acetate nanoparticles in D_2O. Filled diamonds: pure cholesteryl acetate particles, without surfactant. Hollow diamonds: cholesteryl acetate particles with PS-POE as a surfactant, composition ratio $c_S/c_H = 1$ ($c_H = 10^{-3}$ g/g).

The change from Q^{-4} (Fig. 7) to Q^{-2} (Fig. 8) indicates that there is no surfactant in the interior of the particles. The fit to the scattering in this range is obtained with shells that have an average thickness of 24 nm and a standard deviation of the thickness of 5 nm. This thickness is much larger than the thickness of a monolayer of PS-POE molecules, which is calculated to be 8.2 nm for the dispersion at $c_S/c_H = 0.25$ and 3.1 nm for the dispersion at $c_S/c_H = 0.10$. These results show that the adsorbed surfactant does not form a monolayer of uniform thickness, but rather a layer formed of thick and thin patches.

The excess scattering at $Q = 0.3$ nm^{-1} is observed in the dispersions that contain a large excess of surfactant (Fig. 8); an obvious interpretation is that this scattering originates from surfactant micelles that are in water. Indeed, the average molar mass of these micelles, measured through gel permeation chromatography, is 300000 g/mol. From this value, the aggregation number is calculated to be 150 PS-POE molecules, and the radius of the PS core is calculated to be 3.9 nm. This is in good agreement with the size of the small spheres used in the fit of the scattering curve (the water swollen POE shell would contribute only at smaller Q values).

In summary, the surfactant is located in irregular monolayers covering the particles and in small micelles that are dispersed in water.

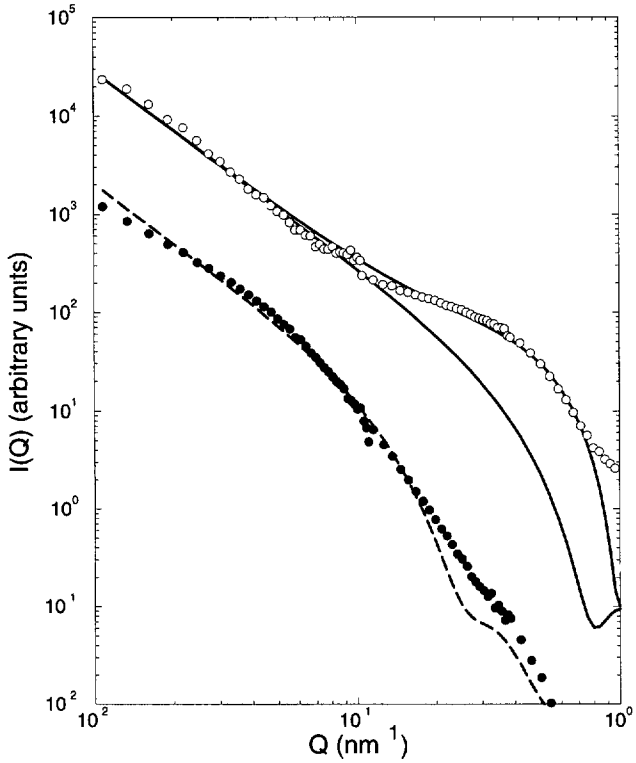

Fig. 8. — Scattering curves of dispersions containing PSD nanoparticles covered with PS-POE as a surfactant, in D_2O. Hollow circles: Taking final concentrations equal to 5×10^{-4} g/g for both PS-POE and PSD ($c_S/c_H = 1$); THF, 0.1 g/g. The full lines correspond to the calculated scattering curves for a dispersion containing large shells (outer diameters beyond, thickness 24 nm, standard deviation on thickness, 5 nm) and small micelles (diameter 7.6 nm). Filled circles: Concentrations equal to 5×10^{-4} g/g and 10^{-2} g/g for PS-POE and PSD, respectively ($c_S/c_H = 0.05$); THF, 0.1 g/g. The dashed line corresponds to the calculated scattering curve for a dispersion containing large shells (outer diameters beyond 175, thickness 24 nm, standard deviation on thickness, 5 nm).

5. Numerical Simulations of the Growth Poisoning

5.1. THE MODEL. — Numerical models for droplets growing by coalescence have been introduced previously [24], however, the poisoning mechanism have not been accounted for in these models. In the following, we introduce a lattice model to simulates a growth poisoning mechanism as exhibed by our experimental system.

5.1.1. The System. — We have considered lattice sites limited in a cubic box of edge length L. Two particle species H (hydrophobic molecule) and S (surfactant) are considered. For the starting configuration, time $t = 0$, a number N_H of particles H and N_S of particles S, each one of a cubic site size of unit length, are distributed randomly and uniformly in the box, avoiding overlaps. Each particle is then a unit cell containing six faces of unit area. Concentration, or volume fraction, of species are related to N_S and N_H by:

$$c_H = \frac{N_H}{L^3} \tag{6a}$$

$$c_S = \frac{N_S}{L^3}. \tag{6b}$$

In our algorithm we introduce a time parameter τ to include a time delay in which surfactant (S specie) adsorption by cluster i_H (formed by one ore more particles of the H species) becomes possible.

5.1.2. The Algorithm. — The algorithm consists in an iterative procedure, in which at a given iteration a cluster i_H or a surfactant i_S is picked up at random (under the assumption that its diffusion coefficient is proportional to n^α, α is the kinetic exponent equal to $-\frac{1}{3}$ for a 3-dimensional compact system of n particles), according to probability distributions, for H species:

$$p_{i_H} = \frac{n_{i_H}^\alpha}{\sum_{j_H} n_{j_H}^\alpha + n_S} \tag{7a}$$

and for S species

$$p_{i_S} = \frac{1}{\sum_{j_H} n_{j_H}^\alpha + n_S} \tag{7b}$$

where n_S is the number of free surfactants. Then, a displacement of a unit step is tried by choosing at random a direction among the six possibilities $(\pm 1, 0, 0)$, $(0, \pm 1, 0)$, $(0, 0, \pm 1)$, taking care of periodic boundary conditions (PBC). If the moving object does not try to occupy a site occupied by other object, the displacement is performed. In the opposite case, no displacement is performed and: (i) if the collision is between a free surfactant and a surface site of specie H (belonging to a cluster i_H), a bond is established between them provided the time t is larger than τ, and the mass n_{i_H} of the cluster i_H is incremented by one. (ii) if the collision takes places between two (or more) sites (H or S species) belonging to two (or more) different clusters, and each one with at least one free surface site, we proceeds to the "coalescence" of the clusters by arranging the new mass $(= n_{i'_H} + n_{i''_H} + ..)$ in a compact configuration with minimum surface. Then, we arrange on the new surface the total number of surfactants $i_{S'} + i_{S''} + ..$ adsorbed previously by the coalescing clusters. If this number exceeds the new surface, the exceeding surfactants are again distributed randomly in the empty sites of the box. (iii) no change is made if the collision is between a free surfactant and another surfactant (even if its has been adsorbed by the surface of a given cluster).

After considering one of the above situations, the algorithm goes on by choosing randomly another cluster or surfactant. The simulation is stopped at a given time t_{end} in which all clusters are saturated in surface by the poisoning effect, or if there is no more than one cluster in the box. According to (7) the time t is calculated adding:

$$\delta t = \frac{1}{\sum_{j_H} n_{j_H}^\alpha + n_S} \tag{8}$$

at each iteration.

As the experiments described above, our numerical calculations have been addressed in the diluted regime, *i.e.* when $c_H + c_S < c_p$ (c_p is the percolation threshold). All results reported below have been calculated at the end of the growth process ($t = t_{end}$).

5.1.3. Two-Dimensional Illustration. — We show in Figure 9 a two-dimensional representation of configurations obtained with our algorithm at three different stages of the process. For $t = 0$, H (depicted in grey, or white when a cluster is saturated) and S (black sites) species are distributed randomly in the box. For $0 < t < t_{end}$ some clusters have been formed by coalescence, and we observe that some of them are fully saturated in surfaces by surfactants,

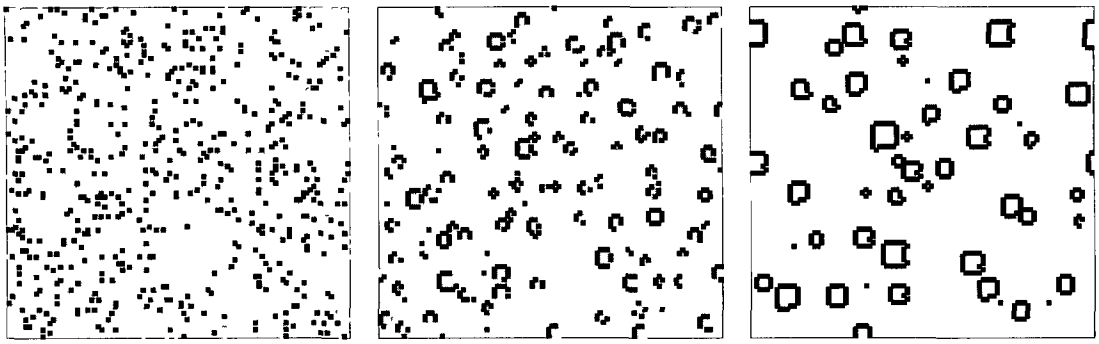

Fig. 9. — Two-dimensional illustration of the growth poisoning for $c_H = 0.06$, $c_S = c_H$ and $L = 100$, at three different stages of the process: for $t = 0$ (left), for $0 < t < t_{end}$ (center), and for $t = t_{end}$ (right). Surfactant species (S) are depicted in black. The particles (or clusters) of hydrophobic species (H) partially saturated by S species are depicted in grey, while they are depicted in white for fully saturated particles (or clusters).

while other surface clusters are partially saturated. At this stage, even if there remains a lot of free surfactants, the surfactant adsorption becomes hard because a given surfactant must explore an important number of surface sites in order to find an available surface site. For $t = t_{end}$ the system reaches a stationary state since all clusters have saturated surfaces, impeding additional coalescence. Note that at this stage there remains some free surfactants. In fact, we will show later that the concentration of the remaining free surfactants depends strongly on the ratio c_S/c_H.

5.2. Results

5.2.1. The Average Cluster Volume Versus the Poisoning Ratio. — In our three-dimensional numerical simulation, we have calculated the average cluster volume using:

$$V_{av} = \frac{N_H}{n_{cl}} \tag{9}$$

where n_{cl} is the number of saturated clusters. In Figure 10 we show a log-log plot of V_{av} *versus* the poisoning ratio c_S/c_H, for $c_H = 0.001$, $\tau = 0$ and three different box sizes $L = 50$ (circle symbols), $L = 80$ (black diamonds) and $L = 110$ (triangle symbols), and for $\tau = 5000$ and $L = 80$ (open diamonds). This figure shows that the average volume V_{av} of the final clusters decreases with increasing poisoning ratio c_S/c_H according to a succession of two power laws. The first power law has an exponent -2.5, then there is a crossover at $\frac{c_S}{c_H} \approx 4$ ($\tau = 0$) to a slower decay, with an exponent -1.3. Interestingly, when there is a delay in the adsorption of surfactants, *i.e.* $\tau = 5000$, the crossover occurs at smaller values of c_S/c_H , but the exponent remains the same. In the following we discuss the absolute magnitudes of the cluster sizes, and the way in which the surfactants are used to control these sizes.

5.2.2. Finite Box Size and Lattice Effects. — In the curves of Figure 10, the smallest c_S/c_H value corresponds to the case in which all clusters have coalesced in a single cluster of volume $V_{av} = N_H$. The corresponding *plateau* for smaller values of c_S/c_H is not shown in the figure since it corresponds just to finite size effects, generally irrelevant for realistic applications. Also, as deduced from the increasing box size L, this c_S/c_H value should tend to zero, when $L \to \infty$.

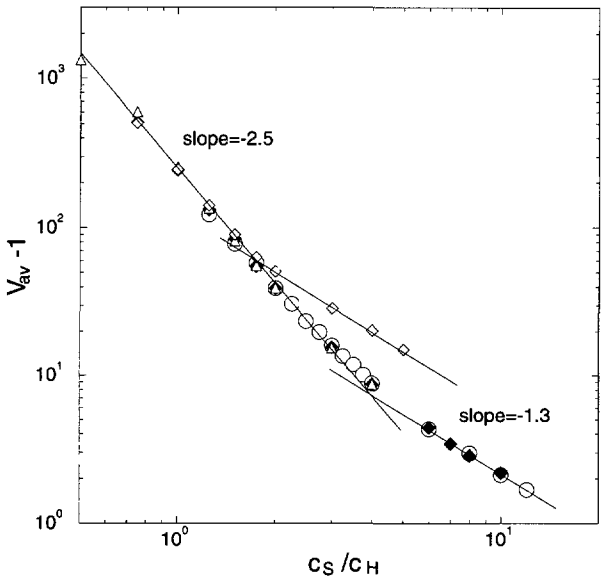

Fig. 10. — log-log plot of the quantity $V_{av} - 1$ *versus* the poisoning ratio c_S/c_H, for $c_H = 0.001$, $t = t_{end}$, and for three different box sizes: $L = 50$ (circles), $L = 80$ (diamonds) and $L = 110$ (triangles). The corresponding time delay values are $\tau = 5000$ for the hollow diamonds ($L = 80$), while in the other curves we considered $\tau = 0$. The full lines correspond to the different power law domains that best fit our data. All these curves result from an average over 50 simulations.

5.2.3. Use of Surfactants. — The two different power laws observed in Figure 10, give information about how surfactants are used. In fact, in a situation in which all N_S surfactants are adsorbed by the cluster surfaces, the possible maximum number of saturated surfaces s^* should be equal to N_S, since, in general, each surfactant can saturate only one face particle of unit area. Therefore, a normalized poisoned cluster surface $\tilde{s}$ could be defined by:

$$\tilde{s} = \frac{s}{s^*} \tag{10}$$

where s is the number of unit area poisoned cluster surfaces. Note that, this quantity is exactly equivalent to the per cent ratio of adsorbed surfactants and is indeed smaller than unity. Furthermore, one has for distributions with well defined average size:

$$\frac{s^*}{n_{cl}} = \frac{N_S}{n_{cl}} \propto V_{av}^{2/3} \tag{11}$$

that combined with (9) gives:

$$V_{av} \propto \left(\frac{c_S}{c_H}\right)^{-3} \tag{12}$$

Note that the exponent measured in the first regime is close to -3, in contrast to the second regime where it is approximately equal to 1.3. The slight deviation from the exponent -3 at low c_S/c_H may originate from surface roughness and from size polydispersity: both effects increase the contents of the surfactant layers as compared with the contents of the particle cores. Therefore, we can conclude that in the small c_S/c_H values the system is in a "efficient"

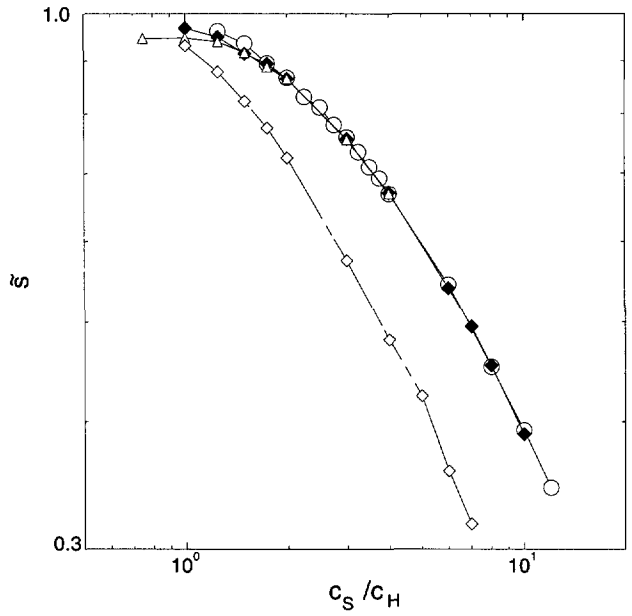

Fig. 11. — log-log plot of the normalized poisoned cluster surface $\tilde{s}$ *versus* the poisoning ratio c_S/c_H. The parameters and legends are the same that Figure 10.

regime of use of surfactants, in contrast to the observed "wasteful" regime at large c_S/c_H values, where the percentage of adsorbed surfactants decreases very quickly.

This is corroborated in Figure 11 where we show a plot of $\tilde{s}$ *versus* c_S/c_H for same parameters as in Figure 10. If all surfactants were adsorbed by the cluster surfaces, $\tilde{s}$ should be equal to one; from our results we note that in the regime of small c_S/c_H values $\tilde{s}$ is close to one, and decreases slowly when increasing c_S/c_H (this conclusion is still more convincing for $L = 110$). In contrast, for large c_S/c_H values, $\tilde{s}$ decreases very quickly when increasing c_S/c_H, and the results for the different box sizes are practically superimposed.

The effect of a time delay τ between aggregation and adsorption is also shown in Figure 11. The corresponding curve (open diamonds) is below the curve at $\tau = 0$, indicating that less surfactant can be adsorbed on the particles and more is wasted. The crossover to the wasteful regime occurs at lower c_S/c_H than that observed in Figure 10: this is because the normalized surface $\tilde{s}$ is strongly dependent on the size distribution function of the system (in contrast to the quantity V_{av} as defined from equation (9)) and, as we will show later, the shape of this function becomes broader when increasing τ.

5.2.4. Competition Between Poisoning and Coalescence. — In this section we examine the kinetic features of the competition between coalescence and poisoning. For this purpose, we vary the initial concentration c_H of hydrophobic molecules, and maintain a high poisoning ratio $c_S/c_H = 4$. We show in Figure 12 how in all cases V_{av} increases when c_H increases for $\tau = 0$ (circles), $\tau = 500$ (squares) and $\tau = 2500$ (triangles). In these simulations the variation of c_H (and c_S) was obtained by considering a fixed number of hydrophobic molecules $N_H = 750$ (and surfactants $N_S = 4N_H$), and varying the box size L as calculated from equation (6). With increasing τ, the average cluster volume V_{av} increases more and more quickly with c_S, these two quantities become proportional, as in a diffusion limited growth mechanism [11,12].

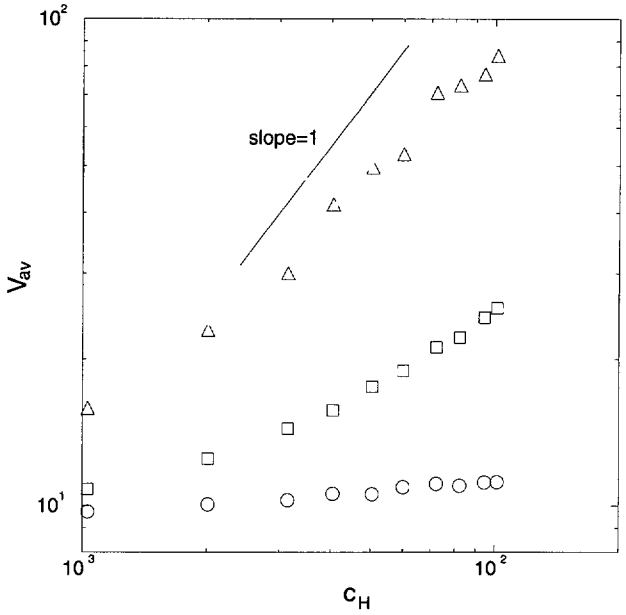

Fig. 12. — log-log plot of the average particle volumes V_{av} *versus* the concentration c_H, for a constant poisoning ratio $c_S/c_H = 4$, and different time delay values: $\tau = 0$ (circles), $\tau = 500$ (squares) and $\tau = 2500$ (triangles). For comparisons the slope 1 is indicated by the full line. All these curves result from an average over 30 simulations.

In fact, for large τ values the $V_{av} \propto c_H$ relation reflects mainly the initial stage of the growth mechanism where surfactant adsorption is forbidden.

To explain these results we have calculated the ratio s_p/s_c between the surfaces loss by poisoning, s_p, where:

$$s_p = \frac{1}{N_S} \int_0^{t_{end}} s_p(t) dt \tag{13a}$$

and the surfaces loss by coalescence:

$$s_c = 1 - s_p. \tag{13b}$$

Figure 13 shows s_p/s_c as function of c_H for the three different τ values and for a constant poisoning ration $c_S/c_H = 4$. The decrease of s_p/s_c at $\tau = 2500$ when c_S increases reflects the loss of surface by coalescence during the delay τ. The slight decrease of s_p/s_c at $\tau = 0$ when c_H increases reflects the fact that, in our model, coalescence is only diffusion limited, whereas surfactant adsorption is reaction limited. Indeed, at long times, a given surfactant spends more time exploring the surface of a cluster to find an avalaible surface site than performing a displacement to reach a cluster. Thus the increase of c_H favors coalescence more than adsorption, since the distances between clusters becomes shorter.

5.3. Size Distributions. — We examine in this section the dependence on the poisoning ratio c_S/c_H and the time delay τ of the size (or volume) distributions. In Figures 14 we show the number n_V of particles of volume V *versus* V for $\tau = 0$ and two different poisoning ratios c_S/c_H equal to 2 (black circles) and 4 (hollow circles) (see Fig. 14a), and for three different time delay values (see Fig. 14b): $\tau = 0$ (circles), $\tau = 2500$ (squares) and $\tau = 8000$ (triangles).

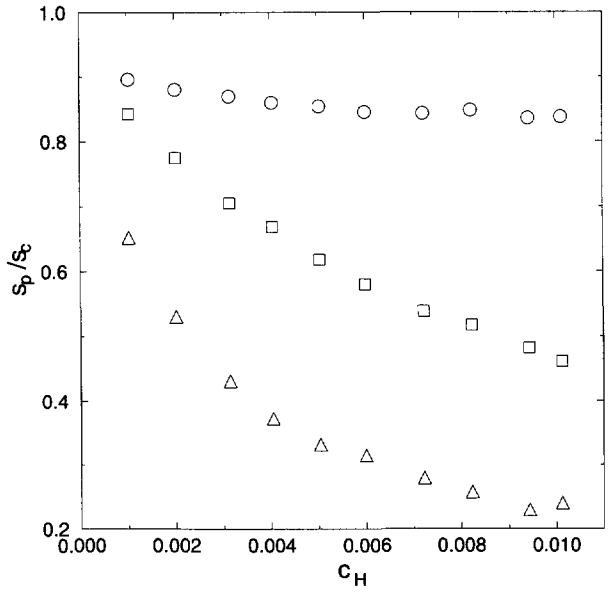

Fig. 13. — Plot of the ratio of the surface lost by poisoning to the surface lost by coalescence s_p/s_c *versus* c_H. The parameters and legends are the same as in Figure 12.

Note that in almost all cases the size distribution function n_V present two maxima, the first corresponds to a monomer peak and the second illustrates the tendency of the system to form particles with a "monodisperse" size distribution. The effect of concentration on the second maximum (illustrated in Fig. 14a) is expected since at low poisoning ratio the average volume should be bigger than at high poisoning ratio, as already observed in Figure 10. In Figure 14b we observe that for $\tau = 8000$ the monomer peak vanishes, this result suggest that at high τ values the system main reflects the aggregation mechanism of a diffusion limited problem, for which it is known that the cluster size distribution is bell shaped, presenting only one maximum [11–13].

The bimodal shape of the size distribution function is also manifested in our experimental system as observed in Figure 3. The small peak at small size values indicates that the coalescence phenomenon is more important in the former bigger particles. These particles grow up to reach a given average size which, as mentioned above, depends on the poisoning ratio. We point out that the resulting bimodal shape observed here is also consistent with the resulting shape of the size distribution in a off-lattice model of droplets growing by coalescence [25].

6. Smoluchowski Approach of the Growth Poisoning

6.1. EQUATIONS. — The main results of the preceding sections can be recovered using kinetic Smoluchowski equations [26] of this growth process. We have first to assume that the fluctuations of the densities (of surfactants and of hydrophobic molecules), can be neglected. Under this assumption, the surrounding of each cluster or surfactant is the same and identical to the average distribution of objects in the system. More precisely, we consider a collection of N_H molecules H, and N_S surfactants S. At a given time, a cluster of H molecules is defined by its size i_H, its radius R_{i_H} (which is as the power 1/3 of its size), the number Σ_{i_H} of available adsorption sites (which is as the power 2/3 of its size), and the number S_{i_H} of surfactants

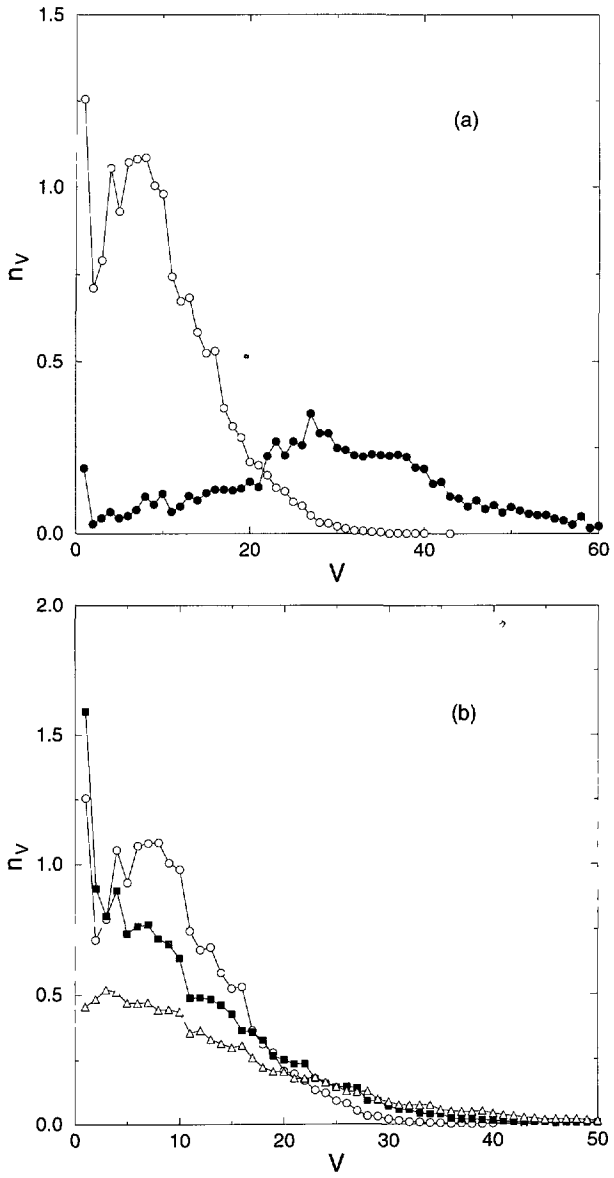

Fig. 14. — Size distribution curves for $C_H = 0.001$ and $L = 50$. In (a) $\tau = 0$, $C_S = 2C_H$ (black circles) and $C_S = 4C_H$ (hollow circles). In (b) $C_S = 4C_H$, $\tau = 0$ (circles), $\tau = 2500$ (squares) and $\tau = 8000$. All these curves results from an average over 2000 simulations.

adsorbed on its surface. At each time step, one investigates all the possible binary events: H + H or H + S, leading to a different state by coalescence or adsorption. A probability weight is attached to each event, namely:

$$K_{i_H,j_H} = \left(\frac{1}{R_{i_H}} + \frac{1}{R_{j_H}}\right)(R_{i_H} + R_{j_H}) \tag{14}$$

for coalescence of two clusters of radii R_{i_H} and R_{j_H}, provided at least one free adsorption site is available on each cluster, and:

$$k_{i_H,S} = \left(\frac{1}{R_{i_H}} + 1\right)(R_{i_H} + 1)\left(1 - \frac{S_{i_H}}{\Sigma_{i_H}}\right) \tag{15}$$

for adsorption of a surfactant (assumed here to be of radius 1). The terms $1/R_{i_H}$ are due to Stokes diffusion, and the $R_{i_H} + R_{j_H}$ are just the cross sections of the clusters during their Brownian path. Then one event is chosen according to these probability weights, and the time is increased by the amount:

$$\delta t = \frac{1}{\sum(K_{i_H,j_H} + k_{i_H,S})}. \tag{16}$$

This leads to the kinetic equations:

$$\frac{\mathrm{d}n_{j,s_j}(t)}{\mathrm{d}t} = \tag{17a}$$

$$\frac{1}{2}\sum_{j',s_{j'},s_{j-j'}} K_{j',j-j'} n_{j',s_{j'}} n_{j-j',s_{j-j'}} - \sum_{j',s_{j'}} K_{j',j} n_{j',s_{j'}} n_{j,s_j} + k_{j,S} n_{j,s_j-1} n_p - k_{j,S} n_{j,s_j} n_p$$

$$\frac{\mathrm{d}n_p(t)}{\mathrm{d}t} = -\sum_{j,s_j} k_{j,S} n_{j,s_j} n_p + \sum_{j',s_{j'},j'',s_{j''}} K_{j',j''} n_{j',s_{j'}} n_{j'',s_{j''}} (s_{j'} + s_{j''} - \Sigma_{j'+j''}). \tag{17b}$$

These equations seem too difficult to be handled analytically. An alternative way to study them is Monte-Carlo simulations: the model is then quite similar to the model described in the preceding section, except that there is no more geometry.

6.2. Results. — The advantage of the Smoluchowski approach is that it is simpler to implement. There is no geometry, so the simulations are fast. Moreover, since one can write down the kinetic equations, analytical investigation can be tempted in simple cases. Nevertheless, this approach is a mean-field theory of the model described in the preceding section, and its validity for ordinary three-dimensional space is not ascertained. This validity has to be checked on the results. In Figure 15, we have plotted the average cluster volume (Eq. (9)) *versus* the poisoning ratio c_S/c_H, for $\tau = 0$, and $N_H = 256$. We see that the two regimes (small- c_S/c_H, for which the surfactants are used efficiently, and large- c_S/c_H, that is excess of surfactants) are well recovered. And we obtain the exponents -2.7 for the small- c_S/c_H values regime, and -1.4 for the other one. Note that these two exponents are slightly larger than those obtained in the Monte Carlo simulations, possibly as a consequence of the absence of geometry in the Smoluchowski approach.

The behaviour of all other computed data are quite similar and are not reproduced here. This shows clearly that the Smoluchowski approach can be used in this process, and that the two regimes meet at about the same point. For example, the ratio of the surface lost by poisoning to the surface lost by coalescence s_p/s_c, obtained from equation (13), decreases with c_H (when aggregation becomes faster) and increases with c_S/c_H (when poisoning becomes more efficient). This last trend is illustrated in Figure 16: the rise of s_p/s_c with c_S/c_H is remarkably close to a linear law. This can be explained in the following way. At very low surfactant concentrations, most of the initial surface is lost by coalescence, therefore $s_c \simeq aN_H$ where a is the number of surface sites in an H molecule (here, we choose $a = 6.5$ to match the values of number of surface sites in the geometrical algorithm for cluster sizes up to 3). All surfactants are used to

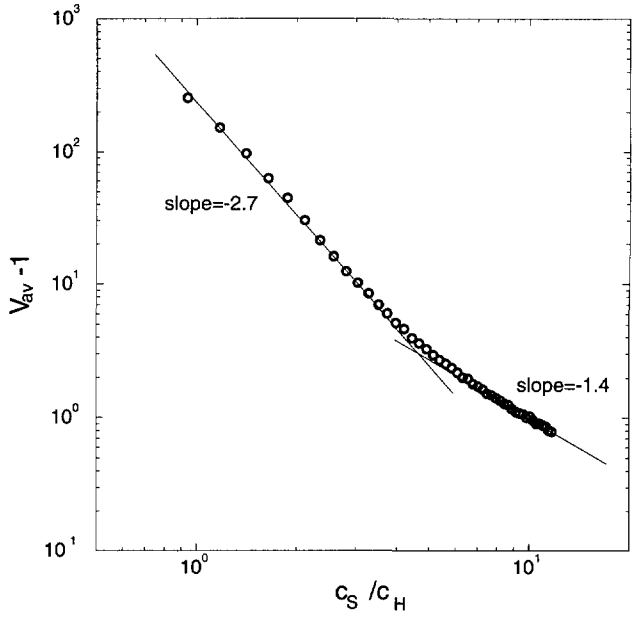

Fig. 15. — log-log plot of the quantity $V_{av} - 1$ *versus* the poisoning ratio c_S/c_H obtained from the Smoluchowski numerical calculations. We considered $N_H = 256$ and $\tau = 0$. The full lines correspond to the different power law domains that best fit our data. This curve result from an average over 1000 simulations.

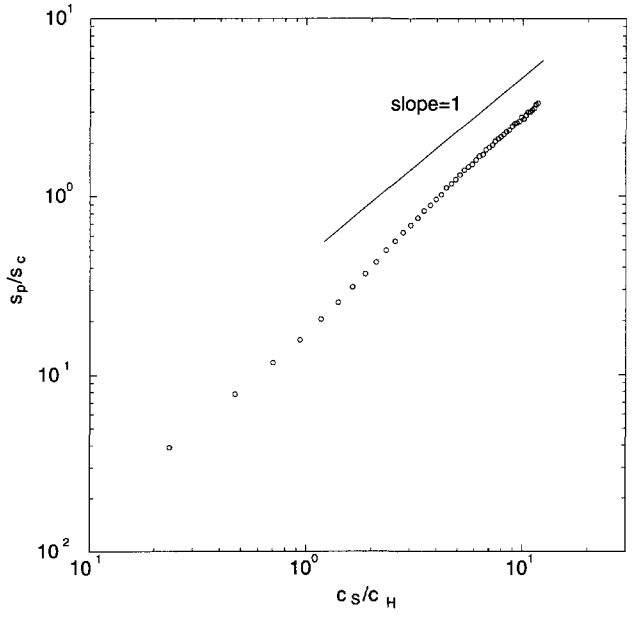

Fig. 16. — Plot of the surface lost by poisoning to the surface lost by coalescence s_p/s_c *versus* the poisoning ratio c_S/c_H obtained from the Smoluchowski numerical calculations. The full line indicates the slope 1.

stop aggregation, therefore $s_p \simeq N_S$. Thus,

$$\frac{s_p}{s_c} \simeq \frac{N_S}{aN_H} \simeq \frac{c_S}{c_H} \tag{18}$$

At very high surfactant concentration, the hydrophobic molecules never form clusters containing more than 2 molecules. In this limit the probability of forming an H–H bond is proportional to c_H, while that of forming an H–S bond is proportional to c_S. Therefore the ratio s_p/s_c is again proportional to c_S/c_H. The complete variation of s_p/s_c, shown in Figure 16, demonstrates that aggregation is the dominant process in most practical situations (up to $c_S/c_H = 4$).

7. Discussion

We start this discussion with a brief summary of experimental results. These results are then compared with the results from numerical simulations. Finally, we try to put together a model for the role of the surfactant in precipitation processes.

7.1. Summary of Experimental Results. — The solution precipitation of hydrophobic molecules in conditions where they are completely insoluble yields particles that are amorphous, dense and globular. Stable aqueous dispersions are obtained when the particles are kept apart by adsorbed surfactants or by impurities that function as surfactants. In these stable dispersions, the particle sizes are determined by two parameters: the poisoning ratio c_S/c_H, *i.e.* the ratio of surfactant molecules to hydrophobic molecules, and the dilution ratio c_H, *i.e.* the ratio of hydrophobic molecules to solvent in the original solution.

The variations of particle sizes according to these parameters show that there are 2 regimes, which differ in the way surfactants are used. At very low concentrations of surfactants, the surface area of the particles matches the area of a monolayer of the surfactant, indicating that all surfactant molecules are used to keep particles apart and limit their aggregation. At higher concentrations of surfactant, the surface area of the particles is much less than the area of a monolayer of the surfactant (Fig. 6).

Neutron scattering experiments on dispersions made in this regime reveal that part of the surfactant is adsorbed on the particles, and part of it forms excess micelles in water.

Thus, attempts to reduce the particle sizes by adding increasing amounts of surfactant become inefficient at some point where most of the added surfactant remains in water.

7.2. Comparison of Experiments with Numerical Simulation. — The kinetic model demonstrates the effects of the competition between aggregation of hydrophobic molecules and poisoning by surfactant. The two-dimensional illustration presented in Figure 9 shows qualitative agreement with the experimental results: particles covered with adsorbed surfactant coexist with single molecules, also covered by surfactant, and with excess surfactant. Quantitative results from the 3-dimensional simulation (Figs. 10 and 11) show a regime of efficient use of the surfactant followed by a regime where most surfactant is wasted. Comparison with experiments (Figs. 5 and 6) shows that, in the simulation, the regime of efficient use extends to much higher surfactant concentrations ($c_S/c_H = 4$ instead of 0.04); as a result, the particle volumes have been reduced to extremely low values (taking 1 nm as the diameter of a monomer, $V_{av} \simeq 10$ instead of 10^7 at the crossover). This discrepancy originates from the time delay between aggregation and surfactant adsorption, as explained below.

In the efficient regime of this simulation, it was assumed that surfactant adsorption starts at the same time as the aggregation of hydrophobic molecules. In the experiments, there is a time delay between the two caused by the finite rate at which water diffuses into the solvent that initially contains hydrophobic molecules and surfactants. A similar delay was introduced in

another simulation. At low surfactant concentrations, this simulation yields the same results as the previous one because the initial aggregation leaves enough surface area to bind all the surfactant (Fig. 10). However, at high surfactant concentration, the particle sizes remain above those obtained with no time delay, because the initial aggregation is not prevented by the excess surfactant. Comparison with the experiments shows that the actual time delay is still much larger than that used in the simulations. A simulation in these conditions would have to handle particles of extremely large sizes. Alternatively, the hydrophobic molecule used in the simulation could be rescaled to be an aggregate containing 10^6 molecules.

In the wasteful regime, the experiments show that the average volume per particle increases linearly with concentration (Fig. 4). The numerical simulation reproduces this trend and provides a simple explanation for it. Indeed, the particle volume rises linearly with concentration only in the limit of long delays (Fig. 12). Therefore the rise in the final volume reflects the unimpeded aggregation during the time delay before the beginning of surfactant adsorption. The linear rise with concentration is indeed that expected from the Smoluchowski equation for kinetic aggregation [11].

In conclusion, the results of experiments are well-reproduced by simulation if aggregation is allowed to proceed unimpeded for a time t, and then adsorption of the surfactant starts. At low surfactant concentration, there is, at that point, more than enough surface to adsorb all surfactant molecules; thus aggregation continues until it is limited because all remaining surfaces are poisoned. Thus the surfactant molecules are used efficiently, but the final particle volumes are large. At high surfactant concentrations, adsorption of surfactant stops the aggregation immediately after the time delay for adsorption. Consequently, the aggregation numbers are determined by the length of this time delay and by the rate of aggregation, *i.e.* by the concentration of hydrophobic molecules. Adding more surfactant does not change these particle volumes; consequently the excess surfactant is wasted.

7.3. MODEL FOR THE PRECIPITATION PROCESS. — As in any kinetic process, the precipitation of hydrophobic molecules in water can be divided into three stages: initiation, propagation and termination.

Initiation is caused by the mixing of water with the solution containing the hydrophobic molecules and surfactant. Immediately, the hydrophobic molecules aggregate, because they are insoluble in this mixed solvent. At this stage, however, the surfactants do not bind to the growing aggregates, because they are not sufficiently hydrophobic.

Propagation proceeds through random collisions of the growing aggregates. According to the Smoluchowski equation, the average volume grows linearly with time, at a rate that is proportional to the concentration of hydrophobic molecules.

Termination occurs when the water content is so high that the surfactants adsorb on the particles. The time delay between aggregation and termination sets the final size of the particles.

In practical situations, it is usually desired to obtain dispersions that are as fine as possible. The results described above set severe limitations for this endeavour. Increasing the surfactant concentration beyond the amount needed to cover the particles at the end of the aggregation stage will not be efficient, since the excess surfactant will just be wasted. Diluting the initial solution will reduce the rate of aggregation, and therefore the particle sizes; however, the final dispersion may be so dilute that it will be necessary to reconcentrate it, which may cause further aggregation. Reducing the time delay between aggregation and adsorption of surfactant requires a device that achieves instantaneous mixing of water and polar solvent. If a high pressure homogenizer could be adapted to achieve this instantaneous mixing, it would be the most attractive option.

Acknowledgments

This work used the neutron beams of ILL in Grenoble, France. It was performed as part of the BIOAVENIR program financed by RHONE-POULENC with the MRE and MICE. One of us (A.H.) would like to acknowledge support from CONICIT (Venezuela) and CNRS (France).

References

[1] Puisieux F., Barratt G., Couarraze P., Couvreur P., Devissaguet J.P., Dubernet C., Fattal E., Fessi H., Vauthier C. and Benita S., *Polym. Biomater.* (1994) 749.
[2] Al-Angary A. and Halbert G. W., *Drug Targeting Delivery (Microencapsulation of drugs)* **1** (1992) 277.
[3] Allemann E., Gurny R. and Doelker E., *Eur. J. Pharm. Biopharm.* **39** (1993) 173.
[4] Gregoriadis G., Liposomes as drug carriers (Wiley, 1988).
[5] Julienne M.C., Alonso M.J., Gomez Amoza J.L. and Benoit J.P., *Drug Dev. Ind. Pharmacy* **18** (1992) 1063.
[6] Koosha F. and Muller R.H., *Archiv. Pharm.*, suppl. **321** (1988) 680.
[7] Sjöström B., Kaplun A., Talmon Y. and Cabane B., *Pharm. Res.* **12** (1995) 39.
[8] Spenlehauer G., Vert M., Benoit J.P., Chabot F. and Veillard M., *J. Controlled Rel.* **7** (1988) 217.
[9] Alkhouri-Fallouh N., Roblot-Treupel L., Fessi H., Devissaguet J.P. and Puisieux F., *Int. J. Pharmaceut.* **28** (1986) 125.
[10] Stolnik S., Davies M.C., Illum L., Davis S.S., Boustta M. and Vert M., *J. Controlled Rel.* **30** (1994) 57.
[11] Jullien R. and Botet R., Aggregation and Fractal Aggregates (World Scientific, Singapore, 1987).
[12] Meakin P., Phase Transitions and Critical Phenomena, vol. 12 (Academic Press, New York, 1988) p. 335.
[13] Vicsek T., Fractal Growth Phenomena (World Scientific, Singapore, 1989).
[14] Wendorf J.H. and Price F.P., *J. Phys. Chem.* **75** (1971) 18.
[15] Wendorf J.H. and Price F.P., *Mol. Cryst. Liq. Cryst.* **25** (1974) 71.
[16] Kunihisa K.S. and Gotoh M., *Mol. Cryst. Liq. Cryst.* **42** (1977) 97.
[17] Cotton J.P., Neutrons, X-rays and Ligth Scattering, P. Linder and Th. Zemb, Eds. (Elsevier Science Publishers, 1991) p. 3.
[18] Strazielle C. and Weill G., Analyses chimiques et caractérisations, Techniques de l'Ingénieur P1, pp. 1065-1–1065-22.
[19] Cabane B., Surfactants solutions: new methods of investigations, Surfactants Sciences Series, R. Zana, Ed., vol. 22 (Marcel Dekker Inc., New York, 1987) p. 57.
[20] Bellare J.R., Davis H. T., Scriven L. E. and Talmon Y., *J. Electron Microx. Technique* **10** (1988) 87.
[21] Lichterfeld F., Schmeling T. and Strey R., *J. Phys. Chem.* **90** (1986) 5762.
[22] Olsson U., Würz U. and Strey R., *J. Phys. Chem* **97** (1993) 4535.
[23] Sonneville O., private communication.
[24] for a review see: Meakin P., *Rep. Prog. Phys.* **55** (1992) 157.
[25] Family F. and Meakin P., *Phys. Rev. A* **40** (1989) 3836.
[26] van Dongen P.G.J. and Ernst M.H., *J. Stat. Phys.* **50** (1988) 295.